

Hydrodynamic attractors, initial state energy and particle production in relativistic nuclear collisions

Giuliano Giacalone*

Institut de physique théorique, Université Paris Saclay, CNRS, CEA, F-91191 Gif-sur-Yvette, France

Aleksas Mazeliauskas†

Institut für Theoretische Physik, Universität Heidelberg, D-69120 Heidelberg, Germany

Sören Schlichting‡

Fakultät für Physik, Universität Bielefeld, D-33615 Bielefeld, Germany

(Dated: August 9, 2019)

We exploit the concept of hydrodynamic attractors to establish a general relation between the initial state energy and the produced particle multiplicities in high-energy nuclear collisions. When combined with an ab initio model of energy deposition, the entropy production during the pre-equilibrium phase naturally explains the universal centrality dependence of the measured charged particle yields in nucleus-nucleus collisions. We further estimate the energy density of the far-from-equilibrium initial state and discuss how our results can be used to constrain non-equilibrium properties of the quark-gluon plasma.

Introduction.— Understanding the equilibration of isolated quantum systems is a fundamental question that touches physical phenomena across vastly different energy scales, from micro kelvin temperatures in cold atom experiments to trillion kelvin temperatures in the dense strong-interaction matter produced in ultra-relativistic nuclear collisions [1–4]. One outstanding discovery made in the field of heavy-ion collisions is that the system created about 1 fm/c ($\approx 3 \cdot 10^{-24}$ s) after the impact of two relativistic nuclei can be described as a deconfined plasma of quarks and gluons (QGP) with macroscopic properties of temperature and velocity [5–8]. Such “unreasonable effectiveness of hydrodynamics” in describing the violent expansion of the QGP droplets triggered a new research area in mathematical physics devoted to the study of *hydrodynamic attractors*, that emerge in out-of-equilibrium systems experiencing very fast memory loss of initial conditions and exhibiting a universal approach towards thermal equilibrium [9, 10].

In this article we show that hydrodynamic attractors can be used to describe entropy production in relativistic nuclear collisions and to make robust estimates of initial-state energy *before* the onset of equilibration. We derive a simple formula, Eq. (6), that relates the energy density of the initial state to the measured charged particle multiplicity, $dN_{\text{ch}}/d\eta$, and point out two important phenomenological consequences of this result. We show that the universal centrality dependence of $dN_{\text{ch}}/d\eta$ across a wide range of collision systems can be naturally reproduced by combining the initial-state energy deposition in high-energy quantum chromodynamics (QCD) with the non-linear entropy production during the equilibration process. Secondly, we determine the initial energy per unit space-time rapidity, $dE_0/d\eta_s$, for different collision centralities at the Relativistic Heavy-Ion Collider (RHIC) and the Large Hadron Collider (LHC). By comparing our

results to the experimentally measured dE_{final}/dy in the final state, we estimate the work performed during the expansion of the system [11] and discuss how such an analysis constrains non-equilibrium and transport properties of the QGP.

Hydrodynamic attractors & Entropy production.— We describe the early time dynamics ($\tau \lesssim 1$ fm/c) of the high-temperature QCD plasma created in high-energy heavy-ion collisions by the out-of-equilibrium evolution of a boost-invariant and transversely homogeneous conformal system [12]. Energy-momentum conservation dictates that the energy density, $e = T^{\tau\tau}$, evolves according to

$$\partial_\tau e = -\frac{e + P_L}{\tau}, \quad (1)$$

where $P_L \equiv \tau^2 T^{\eta_s \eta_s}$ is the longitudinal pressure and we use proper time $\tau \equiv \sqrt{t^2 - z^2}$ and space-time rapidity $\eta_s \equiv \text{atanh } z/t$ coordinates. In (local) thermal equilibrium, the longitudinal pressure is directly related to the energy density via an equation of state, e.g. $P_L = e/3$ for a conformal system. While for small deviations around equilibrium the longitudinal pressure is determined by hydrodynamic constitutive relations in terms of the gradient expansion $P_L/e = \frac{1}{3} - \frac{16}{9} \frac{\eta/s}{\tau T}$, where η/s is the specific shear viscosity [9, 10], this is generally not the case far from equilibrium, where, for instance, at early times after the collision of heavy nuclei the system is highly anisotropic $P_L \ll e$ [4]. Nevertheless, new insights from microscopic equilibration studies [13–26] point to the existence of a hydrodynamic attractor [13], where the far-from-equilibrium system displays an effective constitutive equation $P_L/e = f(\tilde{w})$ well before reaching local thermal equilibrium. Such attractor behavior has been established for a number of different microscopic theories (QCD Kinetic Theory [22–25], Boltzmann RTA [15–

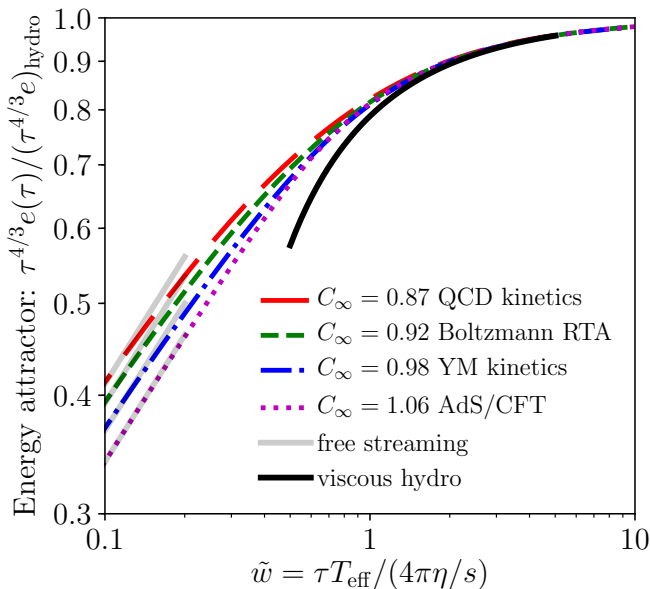


FIG. 1. Hydrodynamic attractor for pre-equilibrium evolution of the energy density obtained from QCD and Yang Mills (YM) kinetic theory [22–25], AdS/CFT [13, 14] and Boltzmann RTA [15–18]. Solid lines show the asymptotic behavior of the attractor curves given by Eq. (4).

[18] and AdS/CFT [13, 14]), where the time evolution on the attractor is controlled by a single scaling variable, $\tilde{w} = \tau T_{\text{eff}}(\tau)/(4\pi\eta/s)$, where $T_{\text{eff}}(\tau)$ is an effective temperature such that $e(\tau) \equiv \frac{\pi^2}{30} \nu_{\text{eff}} T_{\text{eff}}^4(\tau)$.

Based on these insights, the conservation law in Eq. (1) can be integrated, yielding a universal relation between the initial state energy density e_0 at very early times $\tilde{w}(\tau_0) \ll 1$, and the energy density $e(\tau_{\text{hydro}})$ of the near thermal system at later times $\tilde{w}(\tau_{\text{hydro}}) \gg 1$

$$e(\tau_{\text{hydro}}) = e_0 \exp\left(-\int_{\tilde{w}_0}^{\tilde{w}_{\text{hydro}}} \frac{d\tilde{w}}{\tilde{w}} \frac{1+f(\tilde{w})}{\frac{3}{4}-\frac{1}{4}f(\tilde{w})}\right). \quad (2)$$

Close to equilibrium $f(\tilde{w}_{\text{hydro}}) \approx 1/3$ and the energy density of the longitudinally expanding plasma follows the Bjorken scaling $e(\tau) = e_{\text{hydro}}(\tau/\tau_{\text{hydro}})^{-4/3}$, while the entropy density per unit rapidity, $s\tau$, remains constant [12]. Eventually, for $\tau \gtrsim R/c$, where $2R$ denotes the transverse extent of the system, the QGP fireball starts expanding in the transverse plane and ultimately freezes out in color neutral hadrons [27]. During the transverse expansion the QGP remains close to equilibrium and the total entropy per unit rapidity $dS/d\eta_s = A_\perp (s\tau)_{\text{hydro}}$ (where $A_\perp = \pi R^2$) is approximately conserved onwards from the time τ_{hydro} when the QGP can be described as an almost ideal fluid. Ultimately, on the freeze-out surface $dS/d\eta_s$ becomes proportional to the produced charged hadron multiplicity, $dN_{\text{ch}}/d\eta$. The multiplicity of final-state particles emitted from the QGP is therefore a sensitive probe of the entropy production during the

pre-equilibrium phase.

Strikingly, the correspondence between initial-state energy density and charged hadron multiplicity can be quantified further using the theory of hydrodynamic attractors. By factoring out the late time Bjorken scaling from Eq. (2) the evolution of the energy density during the pre-equilibrium phase can be characterized by an attractor curve $\mathcal{E}(\tilde{w})$ [28]

$$\frac{e(\tau)\tau^{4/3}}{e_{\text{hydro}}\tau_{\text{hydro}}^{4/3}} = \mathcal{E}\left(\tilde{w} = \frac{T_{\text{eff}}(\tau)\tau}{4\pi\eta/s}\right). \quad (3)$$

As can be seen from Fig. 1, the function $\mathcal{E}(\tilde{w})$ smoothly interpolates between an early free-streaming and late-stage viscous hydrodynamics [14, 22]

$$\begin{aligned} \mathcal{E}(\tilde{w} \ll 1) &= C_\infty^{-1} \tilde{w}^{4/9} && \text{(free streaming)}, \\ \mathcal{E}(\tilde{w} \gg 1) &= 1 - \frac{2}{3\pi\tilde{w}} && \text{(viscous hydro)}, \end{aligned} \quad (4)$$

where C_∞ is a constant of order unity. Even though the evolution at intermediate times can be different for different microscopic theories, the overall similarity between different theories is remarkable. Most importantly for our purpose, all curves have the same universal characteristics, Eq. (4), at early and late times, irrespective of the underlying microscopic theory.

Based on Eq. (3), we can immediately establish a quantitative relation between the energy densities $e(\tau)$ at various stages, which upon use of the thermodynamic relations $Ts = e + p$ and $p = e/3$ once the system is close to equilibrium turns into an estimate of the entropy per unit rapidity

$$(s\tau)_{\text{hydro}} = \frac{4}{3} \left(\frac{\pi^2}{30} \nu_{\text{eff}}\right)^{1/4} \left(\lim_{\tau \rightarrow 0} \frac{e(\tau)\tau^{4/3}}{\mathcal{E}\left(\frac{T_{\text{eff}}(\tau)\tau}{4\pi\eta/s}\right)}\right)^{3/4}. \quad (5)$$

Evaluating the limit according to Eq. (4) one arrives at the central result of this paper, namely the relation

$$(s\tau)_{\text{hydro}} = \frac{4}{3} C_\infty^{3/4} \left(4\pi\frac{\eta}{s}\right)^{1/3} \left(\frac{\pi^2}{30} \nu_{\text{eff}}\right)^{1/3} (e\tau)_0^{2/3}, \quad (6)$$

from which one can directly estimate the charged particle multiplicity as discussed above:

$$\frac{dN_{\text{ch}}}{d\eta} \approx \frac{1}{J} A_\perp (s\tau)_{\text{hydro}} \frac{N_{\text{ch}}}{S}. \quad (7)$$

Here $S/N_{\text{ch}} \equiv (dS/dy)/(dN_{\text{ch}}/dy) \approx 6.7\text{--}8.5$ is the entropy per charged particle at freeze-out [29, 30] and $J \approx 1.1$ is a Jacobian factor between particle rapidity y and pseudo rapidity η [31].

Equations (6) and (7) establish a one-to-one correspondence between the initial-state energy per unit rapidity $dE_0/d\eta_s \approx A_\perp (e\tau)_0$ and the charged particle multiplicity $dN_{\text{ch}}/d\eta$. One crucial feature of this result is that

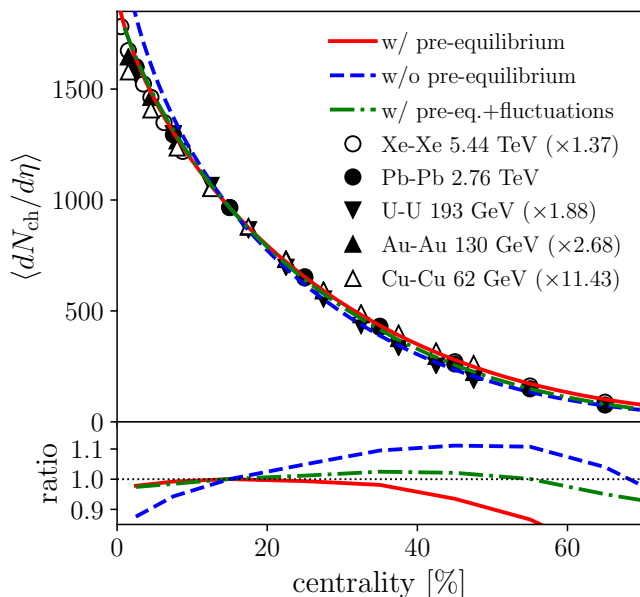


FIG. 2. Top: Centrality dependence of the charged particle multiplicity, $dN_{\text{ch}}/d\eta$, for Xe-Xe [32], Pb-Pb [33], U-U [34], Au-Au [35], and Cu-Cu [35] collisions. Different data points are compared to theoretical results for Pb-Pb collisions, using Eq. (11) (dashed line) and Eq. (12) (solid line), and Eq. (12) within a Glauber Monte Carlo prescription for the thickness functions (dot-dashed line). All curves are normalized to present the same value of multiplicity as ALICE Pb-Pb data in the 10-20% centrality bin. Bottom: Ratio between 2.76 TeV Pb-Pb data and the theory curves.

it accounts for the entropy production during the pre-equilibrium phase, which gives rise to a nontrivial dependence on the initial-state energy density $(e\tau)_0^{2/3}$ as well as on the transport coefficient $(\eta/s)^{1/3}$. Our estimate includes all relevant pre-factors, in particular, the constant C_∞ , which is the property of the hydrodynamic attractor, Eq. (3), and depends on the microscopic physics of equilibration. However it is striking to observe that for the different theories shown in Fig. 1 the variation of C_∞ is only at $\sim 10\%$ level.

Centrality dependence of particle multiplicity.—One important phenomenological consequence of the entropy production in the pre-equilibrium phase concerns the determination of initial conditions for hydrodynamic simulations of heavy ion collisions (see e.g. [36]). While strictly speaking our estimate of the entropy density in Eq. (6) was derived assuming a one dimensional expansion, the influence of transverse gradients can be neglected over the short pre-equilibrium times and we can directly promote Eq. (6) to an estimate for the *local* entropy density, $\tau s(\tau, \mathbf{x}_\perp)|_{\tau=\tau_{\text{hydro}}}$ [37]. Effectively, Eq. (6) then provides a non-linear map of the initial-state energy density profile to the entropy density profile at later times $\tau \sim \tau_{\text{hydro}}$.

Now, in order to illustrate the impact of the pre-

equilibrium phase, we will study the effects on the centrality dependence of the charged particle multiplicity, within a simple initial state model based on the color-glass condensate effective theory of high-energy QCD [38]. Within the dilute-dense formulation of this theory, both the initial energy density per unit rapidity $(e\tau)_0$ as well as the initial gluon multiplicity per unit rapidity $(n\tau)_0$ can be calculated from \mathbf{k}_\perp -factorization, and are given in terms of convolutions of unintegrated gluon distributions [39–43]. Essentially, one finds that (up to logarithmic corrections) $(e\tau)_0$ and $(n\tau)_0$ are proportional to the (local) saturation scales $Q_s(\mathbf{x}_\perp)$ of the two colliding nuclei [39, 40]:

$$(e\tau)_0(\mathbf{x}_\perp) \propto (Q_s^<(\mathbf{x}_\perp))^2 Q_s^>(\mathbf{x}_\perp), \quad (8)$$

$$(n\tau)_0(\mathbf{x}_\perp) \propto (Q_s^<(\mathbf{x}_\perp))^2, \quad (9)$$

where $Q_s^{>/<}$ is the saturation scale of the nucleus representing larger/smaller Q_s at position \mathbf{x}_\perp .

Since the saturation scale locally characterizes the longitudinally integrated density of color charge inside the nucleus, it is generically proportional to the nuclear thickness

$$Q_s^2(\mathbf{x}_\perp) \propto T(\mathbf{x}_\perp), \quad (10)$$

whose definition is recalled in the supplemental material. Based on these considerations, one can then try to estimate the charged particle multiplicity per unit rapidity from the initial gluon multiplicity $(n\tau)_0$ (i.e. w/o pre-equilibrium) according to

$$\frac{dN_{\text{ch}}}{d\eta} \propto \int d^2\mathbf{x}_\perp T^<(\mathbf{x}_\perp), \quad (11)$$

as was done, for example, in [44, 45]. However, such an estimate is appropriate only when there is no significant amount of particle production in the final state. Conversely, if the initial state evolves into an almost ideal QGP fluid, one needs to account for the entropy production during the pre-equilibrium phase. By employing Eqs. (6) and (7) the charged particle multiplicity is then estimated from the initial state energy density $(e\tau)_0$, (i.e. w/ pre-equilibrium) as

$$\frac{dN_{\text{ch}}}{d\eta} \propto \int d^2\mathbf{x}_\perp \left(T^<(\mathbf{x}_\perp) \sqrt{T^>(\mathbf{x}_\perp)} \right)^{2/3}. \quad (12)$$

We illustrate the difference between the two estimates in the upper panel of Fig. 2, where we compare the centrality dependence of the multiplicity $dN_{\text{ch}}/d\eta$ from Eq. (12) (solid line) and Eq. (11) (dashed line), with the nuclear thickness and centrality quantiles determined from the optical Glauber model (see the supplemental material for details). Both estimates are normalized to reproduce the experimentally measured value of $dN_{\text{ch}}/d\eta$ in the 10 – 20% centrality class of Pb–Pb collisions at $\sqrt{s_{\text{NN}}} = 2.76$ TeV. Different trends in the centrality dependence of $dN_{\text{ch}}/d\eta$ are clearly visible, indicating the

importance of the pre-equilibrium phase when comparing observables of this type to experimental data.

Since $dN_{\text{ch}}/d\eta$ is accurately measured in experiment for a wide variety of colliding systems and energies, we can also compare the two estimates directly to experimental data, which are reported as symbols in the upper panel of Fig. 2. It is interesting to note that the average $\langle dN_{\text{ch}}/d\eta \rangle$ as a function of centrality possesses a remarkable degree of universality, such that—up to an overall normalization factor for each collision system—data points for different colliding species (Au, Cu, Pb, U, Xe) at RHIC and LHC energies all collapse onto a single curve to high accuracy. Despite the simplicity of our theoretical estimate, we find that the curve including pre-equilibrium effects provides a rather good description of the experimental data, except for the more peripheral bins, where fluctuations play an important role (see below). Due to the non-trivial geometry dependence in Eq. (12), the calculation including pre-equilibrium dynamics provides a much better description of the data than the estimate in Eq. (11), which is based solely on the initial state.

Even though Eq. (12) can be clearly justified from theoretical calculations, our description is by no means unique. Other phenomenological models [46–50] successfully reproduce the centrality dependence seen in Fig. 2 by introducing various sources of event-by-event fluctuations such as number and positions of participant nucleons, their interaction strength, etc. However, it is important to emphasize in this context that the pre-equilibrium phase also modifies the statistics of fluctuations, such that for the long wavelength perturbations [21, 22]

$$\frac{\delta s_{\text{hydro}}}{s_{\text{hydro}}} = \frac{2}{3} \frac{\delta e_0}{e_0}, \quad (13)$$

which follows from the linearization of Eq. (6). While Eq. (12) over-predicts particle production in peripheral collisions, it is therefore not surprising that one can restore agreement with peripheral data by including event-by-event fluctuations. This is demonstrated by the dot-dashed line in Fig. 2, where the average of the nuclear thickness in Eq. (12) has been determined from a Glauber Monte Carlo model [51] (see the supplemental material for details).

Estimating the initial-state energy density.—So far we illustrated the utility of Eq. (6) for describing entropy production in the pre-equilibrium phase of high-energy heavy-ion collisions. However, an equally important application concerns the inverse problem, namely the estimation of the energy density e_0 of the non-equilibrium state at very early time τ_0 from experimental measurements of hadrons in the final state.

By inverting Eqs. (6) and (7) (and inserting typical values of $dN_{\text{ch}}/d\eta \sim 1600$ and $A_{\perp} \approx \pi R_{\text{Pb}}^2 \approx 138 \text{ fm}^2$) we obtain the following estimate for the initial energy

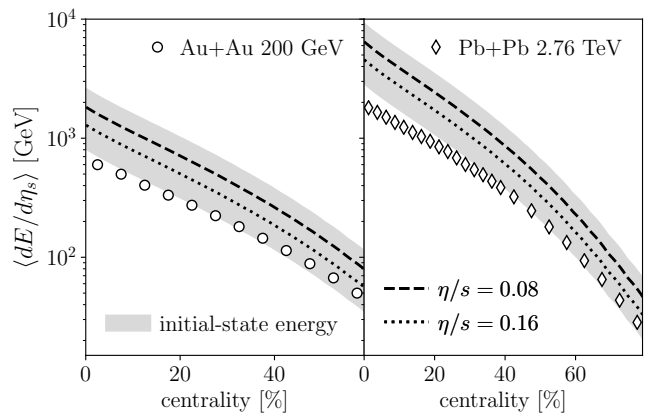


FIG. 3. Estimate of the initial energy per unit space-time rapidity $dE_0/d\eta_s$ (shaded area) determined from the measured particle multiplicity in $\sqrt{s_{\text{NN}}} = 200 \text{ GeV}$ Au-Au (left) and $\sqrt{s_{\text{NN}}} = 2.76 \text{ TeV}$ Pb-Pb collisions (right). Bands correspond to variations of $\eta/s = 0.08$ – 0.24 and $C_{\infty} = 0.80$ – 1.15 while keeping all other parameters fixed as in Eq. (14), and similarly the dashed lines correspond to specific values of $\eta/s = 0.08, 0.16$. For comparison we show data points for the experimentally measured final state energy dE_{final}/dy [31, 34], which is smaller due to the work performed against the longitudinal expansion.

density for central Pb-Pb collisions at $\sqrt{s_{\text{NN}}} = 2.76 \text{ TeV}$:

$$e_0 \approx 270 \text{ GeV/fm}^3 \left(\frac{\tau_0}{0.1 \text{ fm/c}} \right)^{-1} \left(\frac{C_{\infty}}{0.87} \right)^{-9/8} \left(\frac{\eta/s}{2/4\pi} \right)^{-1/2} \left(\frac{A_{\perp}}{138 \text{ fm}^2} \right)^{-3/2} \left(\frac{dN_{\text{ch}}/d\eta}{1600} \right)^{3/2} \left(\frac{\nu_{\text{eff}}}{40} \right)^{-1/2} \left(\frac{S/N_{\text{ch}}}{7.5} \right)^{3/2}, \quad (14)$$

at a time $\tau_0 = 0.1 \text{ fm/c}$, which should be at least of the order of the formation time $1/Q_s \approx 0.1 \text{ fm/c}$ [4], but small compared to the equilibration time $\tau_{\text{hydro}} \approx 1 \text{ fm/c}$ [22, 23] for the estimate in Eq. (14) to be valid [52]. One finds that the initial energy density quoted in Eq. (14) is nearly three orders of magnitude higher than the energy density at the QCD cross-over $e_c \approx 0.346(41) \text{ GeV/fm}^3$ (for 2+1 flavor QCD) [53, 54].

We emphasize that, unlike the usual Bjorken estimate based on the measured final-state energy $e_0 = \frac{1}{\tau_0 A_{\perp}} dE_{\text{final}}/dy$ [12], our estimate in Eq. (14) includes the work done during the expansion of the QGP [11]. We demonstrate this effect in Fig. 3 where we compare the experimentally measured dE_{final}/dy in the final state to the initial-state energy per unit rapidity $dE_0/d\eta_s = \int d\mathbf{x}_{\perp} (e\tau)_0$ reconstructed from the measured particle multiplicities as in Eq. (14). Note that to better account for the non-trivial transverse geometry, we have estimated the transverse area A_{\perp} from our fluctuating initial state model as described in the supplementary material.

Based on this analysis, we find that, especially in central collisions at high energies, the initial state $dE_0/d\eta_s$

can easily exceed the measured dE_{final}/dy in the final state by a factor of two to three. Evidently the exact amount of work done during the expansion is subject to uncertainties in the non-equilibrium and transport properties of the QGP, which we quantify by uncertainty bands in Fig. 3, corresponding to variations of η/s and C_∞ within the anticipated margins ($\eta/s = 0.08\text{--}0.24$ and $C_\infty = 0.80\text{--}1.15$). Vice versa, the size of the uncertainty bands in Fig. 3 also demonstrates the fact that, if the initial state energy density can be determined precisely, e.g. from theoretical calculations, then the experimentally measured $dN_{\text{ch}}/d\eta$ will impose strong constraints on the non-equilibrium evolution of the QGP characterized by C_∞ and η/s . Note that some combinations of parameters, namely large η/s and large C_∞ , can already be ruled out, because the estimated $dE_0/d\eta_s$ in peripheral collisions turns out to be unphysically small, i.e. below the experimental points of dE_{final}/dy , which provide a lower bound on the initial state energy.

Conclusions & Outlook.—Entropy production in high-energy heavy-ion collisions occurs predominantly during the earliest stages, when the system is significantly out-of-equilibrium; therefore measurements of the charged particle multiplicities—reflecting the total amount of entropy produced in the collision—provide a highly sensitive probe of the pre-equilibrium dynamics. Based on the concept of hydrodynamic attractors, which give a macroscopic description of the early time dynamics of the QGP, we established for the first time a direct relation between the initial-state energy and the final-state entropy. This relation, Eq. (6), is remarkably insensitive to the microscopic details of the approach to equilibrium (see Fig. 1).

By use of Eq. (6) we are able to draw direct connections between the pre-equilibrium energy density and the measured particle multiplicities in nucleus-nucleus collisions. We demonstrate that the universal centrality dependence of the measured particle yields from 62 GeV Cu-Cu to 5.44 TeV Xe-Xe collisions can be naturally reproduced by the non-linear dynamics of entropy production starting from the initial energy deposition in high energy QCD. By inverting Eq. (6) we further obtain an estimate of the initial state energy density, Eq. (14), which for central Pb-Pb collisions at LHC energies corresponds to an effective temperature $T_{\text{eff}} \sim 630$ MeV at $\tau_0 = 0.1$ fm/c after the collision—a value that is at least a factor of four above the QCD cross-over temperature of $T_c = 156 \pm 1.5$ MeV [54].

By combining the information from $dN_{\text{ch}}/d\eta$ on entropy production and dE_{final}/dy on the work performed against the longitudinal expansion, we demonstrate that a precise calculation of the initial state energy can impose stringent constraints on the shear-viscosity to entropy density ratio η/s . Since, the $dE_0/d\eta_s$ should always be larger than dE_{final}/dy due to the work performed against the longitudinal expansion, one can rule out certain values in the parameter space, where the ini-

tial $dE_0/d\eta_s$ falls below the experimental data points. From our extraction of $dE_0/d\eta_s$, which is based on a scenario of (nearly-)complete equilibration, we obtain an upper limit for $\eta/s \lesssim 0.4$ for the most favorable choice of all other parameters. Conversely, for $\eta/s \gtrsim 0.4$ we can not expect the QGP to equilibrate in peripheral nucleus-nucleus collisions (see also [26, 55]) and our estimates need to be revised. Non-trivial modifications due to incomplete equilibration will arise in this context, which should be investigated further, for instance by means of the KØMPØST pre-equilibrium package [22, 23, 56]. We expect such effects to become particularly important in collisions of smaller nuclei, e.g., p-A or O-O, which may therefore provide even deeper insights into the fascinating out-of-equilibrium dynamics of the QGP.

Acknowledgments.—We thank A. Andronic, J. Berges, N. Borghini, M. Heller, C. Klein-Bösing, A. Kurkela, T. Lappi, M. Martinez, J.Y. Ollitrault, K. Reygers, C. Schmidt, D. Teaney, and R. Venugopalan for stimulating discussions and P. Romatschke for also providing the AdS/CFT attractor curve. This work was supported in part by the German Research Foundation (DFG) through the Collaborative Research Centres “CRC-TR 211: Strong-interaction matter under extreme conditions” (S.S.) and “SFB 1225: Isolated quantum systems and universality in extreme conditions (ISOQUANT)” (A.M.). We thank the Institute for Nuclear Theory at the University of Washington for its kind hospitality and stimulating research environment.

* giuliano.giacalone@ipht.fr

† a.mazeliauskas@thphys.uni-heidelberg.de

‡ sschlichting@physik.uni-bielefeld.de

- [1] W. Busza, K. Rajagopal, and W. van der Schee, *Ann. Rev. Nucl. Part. Sci.* **68**, 339 (2018), arXiv:1802.04801 [hep-ph].
- [2] T. Schfer and D. Teaney, *Rept. Prog. Phys.* **72**, 126001 (2009), arXiv:0904.3107 [hep-ph].
- [3] A. Adams, L. D. Carr, T. Schfer, P. Steinberg, and J. E. Thomas, *New J. Phys.* **14**, 115009 (2012), arXiv:1205.5180 [hep-th].
- [4] S. Schlichting and D. Teaney, (2019), arXiv:1908.02113 [nucl-th].
- [5] J. Adams *et al.* (STAR), *Nucl. Phys.* **A757**, 102 (2005), arXiv:nucl-ex/0501009 [nucl-ex].
- [6] K. Adcox *et al.* (PHENIX), *Nucl. Phys.* **A757**, 184 (2005), arXiv:nucl-ex/0410003 [nucl-ex].
- [7] B. B. Back *et al.*, *Nucl. Phys.* **A757**, 28 (2005), arXiv:nucl-ex/0410022 [nucl-ex].
- [8] I. Arsene *et al.* (BRAHMS), *Nucl. Phys.* **A757**, 1 (2005), arXiv:nucl-ex/0410020 [nucl-ex].
- [9] W. Florkowski, M. P. Heller, and M. Spalinski, *Rept. Prog. Phys.* **81**, 046001 (2018), arXiv:1707.02282 [hep-ph].
- [10] P. Romatschke and U. Romatschke, *Relativistic Fluid Dynamics In and Out of Equilibrium*, Cambridge Mono-

- graphs on Mathematical Physics (Cambridge University Press, 2019) [arXiv:1712.05815 \[nucl-th\]](#).
- [11] M. Gyulassy and T. Matsui, *Phys. Rev.* **D29**, 419 (1984).
- [12] J. D. Bjorken, *Phys. Rev.* **D27**, 140 (1983).
- [13] M. P. Heller, R. A. Janik, and P. Witaszczyk, *Phys. Rev. Lett.* **108**, 201602 (2012), [arXiv:1103.3452 \[hep-th\]](#).
- [14] P. Romatschke, *Phys. Rev. Lett.* **120**, 012301 (2018), [arXiv:1704.08699 \[hep-th\]](#).
- [15] M. P. Heller, A. Kurkela, M. Spaliski, and V. Svensson, *Phys. Rev.* **D97**, 091503 (2018), [arXiv:1609.04803 \[nucl-th\]](#).
- [16] M. Strickland, J. Noronha, and G. Denicol, *Phys. Rev.* **D97**, 036020 (2018), [arXiv:1709.06644 \[nucl-th\]](#).
- [17] J.-P. Blaizot and L. Yan, *Phys. Lett.* **B780**, 283 (2018), [arXiv:1712.03856 \[nucl-th\]](#).
- [18] M. Strickland, *JHEP* **12**, 128 (2018), [arXiv:1809.01200 \[nucl-th\]](#).
- [19] A. Kurkela and Y. Zhu, *Phys. Rev. Lett.* **115**, 182301 (2015), [arXiv:1506.06647 \[hep-ph\]](#).
- [20] L. Keegan, A. Kurkela, P. Romatschke, W. van der Schee, and Y. Zhu, *JHEP* **04**, 031 (2016), [arXiv:1512.05347 \[hep-th\]](#).
- [21] L. Keegan, A. Kurkela, A. Mazeliauskas, and D. Teaney, *JHEP* **08**, 171 (2016), [arXiv:1605.04287 \[hep-ph\]](#).
- [22] A. Kurkela, A. Mazeliauskas, J.-F. Paquet, S. Schlichting, and D. Teaney, *Phys. Rev.* **C99**, 034910 (2019), [arXiv:1805.00961 \[hep-ph\]](#).
- [23] A. Kurkela, A. Mazeliauskas, J.-F. Paquet, S. Schlichting, and D. Teaney, *Phys. Rev. Lett.* **122**, 122302 (2019), [arXiv:1805.01604 \[hep-ph\]](#).
- [24] A. Kurkela and A. Mazeliauskas, *Phys. Rev. Lett.* **122**, 142301 (2019), [arXiv:1811.03040 \[hep-ph\]](#).
- [25] A. Kurkela and A. Mazeliauskas, *Phys. Rev.* **D99**, 054018 (2019), [arXiv:1811.03068 \[hep-ph\]](#).
- [26] A. Kurkela, U. A. Wiedemann, and B. Wu, (2019), [arXiv:1905.05139 \[hep-ph\]](#).
- [27] D. A. Teaney, in *Quark-gluon plasma 4*, edited by R. C. Hwa and X.-N. Wang (2010) pp. 207–266, [arXiv:0905.2433 \[nucl-th\]](#).
- [28] Note that for a conformal system subject to a transversely homogenous and boost invariant expansion, the hydrodynamic attractor curve is uniquely determined by a single function, such as P_L/e which is the most common choice in the literature. The attractor curve in Eq. (3) is related to the attractor curve for P_L/e by virtue of Eq. (2).
- [29] P. Hanus, A. Mazeliauskas, and K. Reygers, to appear soon.
- [30] P. Hanus, *Entropy in Pb-Pb Collisions at the LHC, Bachelor's thesis*, University of Heidelberg (2018), supervisor Prof. Klaus Reygers.
- [31] J. Adam *et al.* (ALICE), *Phys. Rev.* **C94**, 034903 (2016), [arXiv:1603.04775 \[nucl-ex\]](#).
- [32] S. Acharya *et al.* (ALICE), *Phys. Lett.* **B790**, 35 (2019), [arXiv:1805.04432 \[nucl-ex\]](#).
- [33] K. Aamodt *et al.* (ALICE), *Phys. Rev. Lett.* **106**, 032301 (2011), [arXiv:1012.1657 \[nucl-ex\]](#).
- [34] A. Adare *et al.* (PHENIX), *Phys. Rev.* **C93**, 024901 (2016), [arXiv:1509.06727 \[nucl-ex\]](#).
- [35] B. Alver *et al.* (PHOBOS), *Phys. Rev.* **C83**, 024913 (2011), [arXiv:1011.1940 \[nucl-ex\]](#).
- [36] U. Heinz and R. Snellings, *Ann. Rev. Nucl. Part. Sci.* **63**, 123 (2013), [arXiv:1301.2826 \[nucl-th\]](#).
- [37] Specifically, the pre-flow $v_\perp \sim \tau_{\text{hydro}} \nabla_\perp e/e$ is negligible as long as gradients $\nabla_\perp e/e$ are small on the scale of hydrodynamization time ($c\tau_{\text{hydro}}$) [21, 22] and the one dimensional constitutive relation for P_L/e approximately remains valid, as explicitly confirmed in [26].
- [38] F. Gelis, E. Iancu, J. Jalilian-Marian, and R. Venugopalan, *Ann. Rev. Nucl. Part. Sci.* **60**, 463 (2010), [arXiv:1002.0333 \[hep-ph\]](#).
- [39] A. Dumitru and L. D. McLerran, *Nucl. Phys.* **A700**, 492 (2002), [arXiv:hep-ph/0105268 \[hep-ph\]](#).
- [40] T. Lappi, *Phys. Lett.* **B643**, 11 (2006), [arXiv:hep-ph/0606207 \[hep-ph\]](#).
- [41] J. P. Blaizot, F. Gelis, and R. Venugopalan, *Nucl. Phys.* **A743**, 13 (2004), [arXiv:hep-ph/0402256 \[hep-ph\]](#).
- [42] J.-P. Blaizot and Y. Mehtar-Tani, *Nucl. Phys.* **A818**, 97 (2009), [arXiv:0806.1422 \[hep-ph\]](#).
- [43] J. P. Blaizot, T. Lappi, and Y. Mehtar-Tani, *Nucl. Phys.* **A846**, 63 (2010), [arXiv:1005.0955 \[hep-ph\]](#).
- [44] M. Mace, V. V. Skokov, P. Tribedy, and R. Venugopalan, *Phys. Rev. Lett.* **121**, 052301 (2018), [arXiv:1805.09342 \[hep-ph\]](#).
- [45] B. Schenke, P. Tribedy, and R. Venugopalan, *Phys. Rev.* **C86**, 034908 (2012), [arXiv:1206.6805 \[hep-ph\]](#).
- [46] H. J. Drescher and Y. Nara, *Phys. Rev.* **C75**, 034905 (2007), [arXiv:nucl-th/0611017 \[nucl-th\]](#).
- [47] B. Alver, M. Baker, C. Loizides, and P. Steinberg, (2008), [arXiv:0805.4411 \[nucl-ex\]](#).
- [48] C. Gale, S. Jeon, B. Schenke, P. Tribedy, and R. Venugopalan, *Phys. Rev. Lett.* **110**, 012302 (2013), [arXiv:1209.6330 \[nucl-th\]](#).
- [49] H. Niemi, K. J. Eskola, and R. Paatelainen, *Phys. Rev.* **C93**, 024907 (2016), [arXiv:1505.02677 \[hep-ph\]](#).
- [50] J. E. Bernhard, J. S. Moreland, S. A. Bass, J. Liu, and U. Heinz, *Phys. Rev.* **C94**, 024907 (2016), [arXiv:1605.03954 \[nucl-th\]](#).
- [51] M. L. Miller, K. Reygers, S. J. Sanders, and P. Steinberg, *Ann. Rev. Nucl. Part. Sci.* **57**, 205 (2007), [arXiv:nucl-ex/0701025 \[nucl-ex\]](#).
- [52] Between the two time-scales the evolution of the energy density is characterized by the attractor curve in Fig. 1, which for sufficiently small τ_0 is well approximated by the early time asymptotic in Eq. (4). However, before a time $\tau \sim 1/Q_s$ the energy density per unit rapidity increases as energy deposition still takes place (see e.g. [40, 57]).
- [53] H.-T. Ding, F. Karsch, and S. Mukherjee, *Int. J. Mod. Phys.* **E24**, 1530007 (2015), [arXiv:1504.05274 \[hep-lat\]](#).
- [54] A. Bazavov *et al.* (HotQCD), *Phys. Lett.* **B795**, 15 (2019), [arXiv:1812.08235 \[hep-lat\]](#).
- [55] R. S. Bhalerao, J.-P. Blaizot, N. Borghini, and J.-Y. Ollitrault, *Phys. Lett.* **B627**, 49 (2005), [arXiv:nucl-th/0508009 \[nucl-th\]](#).
- [56] A. Kurkela, A. Mazeliauskas, J.-F. Paquet, S. Schlichting, and D. Teaney, “K \emptyset MP \emptyset ST: linearized kinetic theory propagator of initial conditions for heavy ion collisions,” <https://github.com/KMPST/KoMPoST> (2018).
- [57] G. Chen, R. J. Fries, J. I. Kapusta, and Y. Li, *Phys. Rev.* **C92**, 064912 (2015), [arXiv:1507.03524 \[nucl-th\]](#).
- [58] H. De Vries, C. W. De Jager, and C. De Vries, *Atom. Data Nucl. Data Tabl.* **36**, 495 (1987).
- [59] J. L. Albacete and C. Marquet, *Prog. Part. Nucl. Phys.* **76**, 1 (2014), [arXiv:1401.4866 \[hep-ph\]](#).

Supplementary material

Below we explain the details of the implementation of the initial state model described in the main text. When referring to the optical Glauber calculations, which yield the dashed and solid lines in Fig. 2, we determine the nuclear thickness $T(\mathbf{x}_\perp)$ of each nucleus according to the longitudinal integral of the (average) nuclear matter density distribution $T(\mathbf{x}_\perp) = \int_z dz \rho(\sqrt{\mathbf{x}_\perp^2 - z^2})$. We follow previous works and parametrize $\rho(r)$ by a two-parameter Fermi distribution

$$\rho(r) = \rho_0 \left[1 + \exp\left(\frac{1}{a}[r - R]\right) \right]^{-1}, \quad (15)$$

with $a = 0.55$ fm and $R = 6.62$ fm for ^{208}Pb nuclei, and $a = 0.53$ fm, $R = 6.40$ fm for ^{197}Au nuclei [58], while ρ_0 is such that $\rho(r)$ is normalized to the total number of nucleons. The thickness functions of two nuclei (A and B) colliding at a finite impact parameter, \mathbf{b} , are given by $T^{A/B}(\mathbf{x}_\perp) = T(\mathbf{x}_\perp \pm \mathbf{b}/2)$. The centrality of a given collision is obtained from the geometric relation $centrality = \pi|\mathbf{b}|^2/\sigma_{\text{tot}}$ [27], where σ_{tot} is the total inelastic nucleus-nucleus cross section, and we use $\sigma_{\text{tot}} = 767$ fm² for Pb-Pb collisions, and $\sigma_{\text{tot}} = 685$ fm² in Au-Au collisions.

When referring to fluctuating initial conditions, which yield the dot-dashed line in Fig. 2, we introduce nucleonic degrees of freedom following the Monte Carlo version of the Glauber model [51]. In both colliding nuclei we sample the positions of the nucleons according to $\rho(r)$, which we then shift by $\pm\mathbf{b}/2$ to take into account the finite impact parameter. Subsequently, we determine the *participants* in a black-disk approximation as those nucleons of nucleus A that are located within a distance $\sqrt{\sigma_{\text{nn}}/\pi}$ from at least one nucleon in nucleus B, and vice versa. Here σ_{nn} is the nucleon-nucleon cross-section, which is equal to 4.2 fm² for $\sqrt{s_{\text{NN}}} = 200$ GeV and to 6.4 fm² for $\sqrt{s_{\text{NN}}} = 2.76$ TeV. The thickness $T(\mathbf{x}_\perp)$ of each nucleus is then determined on an event-by-event basis by summing the density profiles of all its participating nucleons, where the density of each participant nucleon is taken as a Gaussian profile of width 0.5 fm.

Explicitly restoring the constants in Eqs. (10) and (8), the saturation scale $Q_s(\mathbf{x})$ of the nucleus is determined as

$$Q_s^2(\mathbf{x}_\perp) = Q_{sp}^2(\sqrt{s})A_p T(\mathbf{x}_\perp), \quad (16)$$

where $Q_{sp}(\sqrt{s})$ and $A_p = \pi R_p^2$ denote the saturation scale and (transverse) size of a proton, and the initial state energy density per unit rapidity is then given by

$$(e\tau)_0(\mathbf{x}_\perp) = \mathcal{N}_e (Q_{sp}^2(\sqrt{s})A_p)^{3/2} T^<(\mathbf{x}_\perp)\sqrt{T^>(\mathbf{x}_\perp)}, \quad (17)$$

where \mathcal{N}_e is a dimensionless proportionality coefficient (see e.g. [39]). By use of Eqs. (6) and (7), the multiplicity

in an event is then given by

$$\begin{aligned} \frac{dN_{\text{ch}}}{d\eta} &= \frac{4}{3J} C_\infty^{3/4} \left(4\pi\frac{\eta}{s}\right)^{1/3} \left(\frac{\pi^2}{30}\nu_{\text{eff}}\right)^{1/3} \frac{N_{\text{ch}}}{S} \\ &\quad \mathcal{N}_e^{2/3} Q_{sp}^2(\sqrt{s})A_p \int d\mathbf{x}_\perp \left(T^<(\mathbf{x}_\perp)\sqrt{T^>(\mathbf{x}_\perp)}\right)^{2/3}, \end{aligned} \quad (18)$$

while the initial-state energy per unit rapidity is simply given by the transverse integral of $(e\tau)_0$ in Eq. (17) as

$$\frac{dE_0}{d\eta_s} = \mathcal{N}_e (Q_{sp}^2(\sqrt{s})A_p)^{3/2} \int d\mathbf{x}_\perp T^<(\mathbf{x}_\perp)\sqrt{T^>(\mathbf{x}_\perp)}. \quad (19)$$

Statistical averages of $\frac{dN_{\text{ch}}}{d\eta}$ and $\frac{dE_0}{d\eta_s}$ at a given centrality percentile are then obtained by sampling many events at the corresponding impact parameter. By matching the multiplicity in Eq. (18) to experimental data, we find that the dimensionless combination of pre-factors

$$\frac{4}{3J} C_\infty^{3/4} \left(4\pi\frac{\eta}{s}\right)^{1/3} \left(\frac{\pi^2}{30}\nu_{\text{eff}}\right)^{1/3} \frac{N_{\text{ch}}}{S} \mathcal{N}_e^{2/3} Q_{sp}^2(\sqrt{s})A_p \quad (20)$$

in Eq. (18) should be equal to 10.8 for 2.76 TeV Pb-Pb collisions 4.8 for 200 GeV Au-Au collisions, which is compatible with the expected increase of the saturation scale $Q_s^2(\sqrt{s}) \propto \sqrt{s}^\lambda$ with $\lambda \approx 0.3$ [59].

Vice versa, to determine the initial state energy per unit rapidity shown in Fig. 3, we can use Eq. (18) for the multiplicity to eliminate the pre-factor $\mathcal{N}_e (Q_{sp}^2(\sqrt{s})A_p)^{3/2}$ from Eq. (19) and express $\frac{dE_0}{d\eta_s}$ in the form of Eq. (14) as

$$\begin{aligned} \frac{dE_0}{d\eta_s} &= \left(\frac{4}{3J}\right)^{-3/2} C_\infty^{-9/8} \left(4\pi\frac{\eta}{s}\right)^{-1/2} \left(\frac{\pi^2}{30}\nu_{\text{eff}}\right)^{-1/2} \\ &\quad A_\perp^{-1/2} \left(\frac{S}{N_{\text{ch}}}\right)^{3/2} \left(\frac{dN_{\text{ch}}}{d\eta}\right)^{3/2}, \end{aligned} \quad (21)$$

where the effective area, A_\perp , is given by

$$\sqrt{A_\perp} = \frac{\left(\int d\mathbf{x}_\perp \left(T^<(\mathbf{x}_\perp)\sqrt{T^>(\mathbf{x}_\perp)}\right)^{2/3}\right)^{3/2}}{\int d\mathbf{x}_\perp T^<(\mathbf{x}_\perp)\sqrt{T^>(\mathbf{x}_\perp)}}. \quad (22)$$

Evaluating Eq. (22) within our Monte-Carlo calculations yields $A_\perp \approx 120$ fm² in central Pb-Pb collisions, which is in fair agreement with the value anticipated in Eq. (14). Note that, while we could have used the experimental data for $dN_{\text{ch}}/d\eta$ to produce Fig. 3, we conveniently make use of the model estimate in Eq. (18) to interpolate between experimental data points; as shown in Fig. 2 the model is within 5% of all experimental data.